POAC'23
Glasgow, UK

Proceedings of the 27th International Conference on
Port and Ocean Engineering under Arctic Conditions
12-16 June, Glasgow, UK

An algorithm for determining the grain geometry from ultrasonic measurements of large-grained temperate ice cores

Jerome A Graves, Ben Lishman, Sevan Harput
[1] School of Engineering, London South Bank University, London, UK

ABSTRACT

Ice is anisotropic: properties, including acoustic velocity, vary depending on the direction in which they are measured. Glacial flow is controlled by this bulk anisotropy, which itself depends on the orientation of grains. Incorporating the effect of this mechanical anisotropy is vital to making ice flow models more accurate and deriving glacial movement in the past. The standard method of viewing the grains is to transport drilled ice cores to facilities to cut them into sections. These sections are analysed to determine the size and orientation of ice crystals in the core. This requires the destruction of most of the sample, which results in an incomplete image of the grains. The sample can also be inadvertently modified in the transportation process. Here, we show an algorithm for recreating grain geometry from ultrasound velocities and points of reflection. We demonstrate this algorithm on 2D images from polarised light microscopy of a deep ice core from Rhonegletscherin in the Swiss Alps, and determine the minimum number of scanning angles needed to recreate the grain geometry of the ice core.

KEYWORDS: Ice; Ultrasonics; Tomography; Anisotropy; Crystallography,

1. INTRODUCTION

One-third of the global average sea level rise since 1993 is attributed to meltwater from ice sheets. The crystal fabric is one of the most critical factors determining the ice sheets' mechanical properties, as the deformation and flow of ice sheets are highly dependent on the orientation of their grains.

Ice is a transversely isotropic material. It has some symmetry along one axis but not along the other two axes perpendicular to that axis. The acoustic properties (such as acoustic impedance and sound velocity) can vary depending on the direction of propagation of the ultrasound waves relative to the axis of symmetry (Kerch et al., 2018a).

The anisotropy of ice can lead to changes in the direction and amplitude of the reflected ultrasound waves, depending on the orientation of the ice crystals relative to the ultrasound probe. When ultrasound waves are propagated through the ice, some of the waves will be reflected back towards the probe, generating reflection data that can be used to study the internal structure of the ice.

Ice is polycrystalline. Ice sheets are formed from condensation and snowfall. This snowfall is initially loosely packed and has a random crystal orientation. Over time, the snowfall compacts into firn ice, an intermediary stage between the surface and glacial ice. The firn recrystallises into larger ice crystals as it compacts. This recrystallisation process continues with depth, increasing the size of individual grains with preferential orientations (Kennedy et al., 2013). The crystals' orientation changes with the glacial flow. The grains are formed by stress and ice deformation, storing historical information on ice sheet flow (Saruya et al., 2022).

Glen's flow law is the basis for most past analyses of ice sheets and glacial flow analyses. However, it does not consider the anisotropic properties of ice. More recently, the anisotropic properties of ice have been incorporated into ice flow models (Gillet-Chaulet et al., 2005;

Placidi et al., 2010). Characterising the ice crystal orientation fabric (COF) will allow improved parameterisation of these anisotropic flow models.

The COF is a crucial element to consider when studying sea ice (Cole, 1998). Sea ice is formed by the freezing of seawater, and during this process, ice crystals grow in different orientations, creating distinct COFs. This fabric plays a fundamental role in determining the physical properties of sea ice, including its strength, deformation behaviour, and thermal conductivity. The COF can impact the way sea ice reacts to external forces like wind and ocean currents. This, in turn, affects the global climate by influencing the amount of sea ice cover and the exchange of heat and gases between the ocean and the atmosphere.

The primary method of retrieving the COF is polarised light microscopy. Ice cores are cut into sections, shaved to a sub-millimetre thickness, and placed between 2 polarising lenses. The anisotropic nature of ice causes differently oriented-ice grains to appear in different colours. The process is labour-intensive and destroys most of the sample, giving only discrete measurements and an incomplete image of the crystalline structure (Durand et al., 2006; Langway et al., 1988).

Ultrasound has been used to derive the COF of ice cores. In (Langway et al., 1988), a semi-automatic ultrasonic wave-velocity measuring device was developed. The ice samples must be manipulated to obtain plane-parallel surfaces for cartesian-based scanning. In (Mikesell et al., 2017), laser ultrasound was used to derive the annual layering of ice cores. In (Hellmann et al., 2021), acoustic velocity was measured around the azimuth of ice cores compared with images of the crystal fabric, with positive results.

There is a multitude of solid-state crystal structures of ice. Over 15 have been discovered, some with computational techniques. The most common and stable form is hexagonal Ice (I_h). It has a hexagonal symmetry with space group $P6_3/mmc$ (Cao et al., 2018). Natural snow and ice have this hexagonal structure. Ice (I_h) forms in layers. The layers have strong hexagonal planar bonding, but the bonds that hold the layers vertically are considerably weaker. Parallel to the hexagonal structure is known as the basal plane, with the direction of layering known as the c-axis. This results in transversely isotropic behaviour. Because of this, acoustic velocity measurements parallel to the basal plane show no change. As the inclination of the ice crystals increases, the velocity parallel to the direction of this inclination is reduced. Perpendicular to the inclination, the velocity is unchanged.

In (Hellmann et al., 2021), this framework (Kerch et al., 2018) was used to predict the ultrasound p-wave velocity in ice cores with known crystal fabrics. Results were positive but with inconclusive results with large-grained ice cores. The Matlab MTex toolbox derived a velocity profile for a given crystal structure. MTex velocity profiles will cause the results to be biased by all the other grains in the 2D volume, as it does not account for the grain geometry.

Here we explored the possibility of using ultrasonic reflections to identify the grain geometry with ice cores with larger grains. We use the MatLab Mtex toolbox and custom software to simulate ultrasonic p-wave beam propagation through a two-dimensional digital facsimile of an ice core. The facsimile is created from images from deep temperate ice (79m) Rhonegletscher in the Swiss Alps made from polarised light microscopy, taken from Hellmann

et al., 2021. We quantify the effect of azimuth resolution, single and multielement ultrasonic transducers with sector scanning and evaluate reflection data. When plotting the reflection data, we use a back projection to improve the velocity assumption.

2. DATA AQUISITION AND METHODS

2.1 Deriving velocities of a monocrystal

The velocity of ultrasonic p-waves through ice and vary significantly depending on the ice's temperature, impurity concentration, porosity and the orientation and inclination of its grains. Here, we assume near-perfect hexagonal ice (I_h) with no impurities.

The seismic anisotropy of ice can be described as a fourth-order elasticity tensor. Due to the symmetry of ice (I_h), eighty-one unknown elements can be reduced to five constraints for a monocrystal. In Kerch et al., 2018, a framework was established to derive the elasticity tensor and seismic velocities across all azimuth and inclination angles of monocrystalline ice.

We use the elasticity tensor C_m calculated from Benet at $T = -10°C$, which has provided the best agreement between calculated and measured data in previous ultrasonic experiments (Diez and Eisen, 2015). The elasticity tensor, crystal shape and symmetry values (table 1) derive the ultrasonic velocity of ice at all orientations and inclinations using the Chistoffel equation(Tsvankin, 2012). This approach is used in the MatLab Toolbox Mtex for crystalographic applications.

$$C_m = \begin{bmatrix} 14.06 & 7.15 & 5.88 & 0 & 0 & 0 \\ 7.15 & 14.06 & 5.88 & 0 & 0 & 0 \\ 5.88 & 5.88 & 15.24 & 0 & 0 & 0 \\ 0 & 0 & 0 & 3.06 & 0 & 0 \\ 0 & 0 & 0 & 0 & 3.06 & 0 \\ 0 & 0 & 0 & 0 & 0 & 3.455 \end{bmatrix} \times 10^9\,\mathrm{Nm}^{-2}$$

Table 1. The symmetry values for Ice (Ih)

Space Group	Crystal symmetry	Laue Class Symmetry
$P6_3/mmc$	D_{6h}	6/mmm

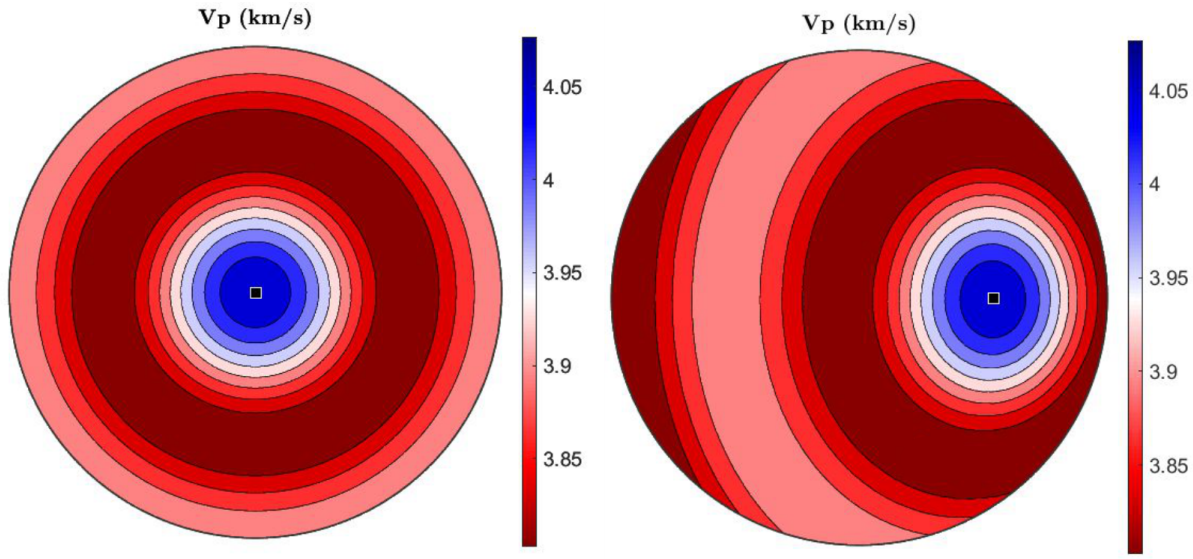

Figure 1. Upper hemisphere plots of the p-wave velocity of an ice monocrystal; left: orientation (0,0,0), right: orientation (45,0,0)

Ice is transversely anisotropic. As seen in Figure 1, parallel to its basal plane, it exhibits isotropic behaviour. It has two maximums; the largest is a singular angle perpendicular to the basal plane, and the other is all the azimuth angles parallel to the basal. The minimum is all the azimuth angles 45 degrees inclined from the basal.

2.2 Converting Ice core polarised light microscopy images into a digital format

We use a polarised light microscopy image from Rhonegletcher, Central Swiss Alps. The ice core was drilled in August 2017 using a thermal drilling technique at a depth of 79m. The diameter of the core is $\approx 70\,\mathbf{mm}$. The orientation of the grains is mostly vertically aligned, with grains partially orientated in the glacial flow direction ($\approx 155^{\circ}$) (Hellmann,Kerch et al., 2021).

Figure 2. The polarised light microscopy image from Rhonegletcher, Central Swiss Alps. The

ice core was drilled in August 2017 using a thermal drilling technique at a depth of 79m.

In order to retain the orientation and inclination of the grains, we utilised computer vision techniques through the OpenCV library to convert the image into a digital format. However, due to the image's resolution, the resulting digital core has a resolution of $0.1\,\mathbf{mm}$.

2.3 Simulating reflection data

When simulating the ultrasonic p-waves, ultrasonic scatter and attenuation are ignored. The beam is modelled as an infinitely thin ray. In previous ultrasound experiments on ice, the optimum frequency was 1MHz (Hellmann,Grab et al., 2021; Simonetti and Fox, 2019).
We start by modelling the transducer as a single-element immersion transducer with a diameter of 13mm. The transducer had a good acoustic impedance match in previous ice ultrasound experiments. Due to the changes in ultrasonic velocity through the ice core, there is no single wavelength for the beam, but we modelled it as approximately 3.85 mm using the mean velocity of the ice core.

In our simulation, we generate reflection data by examining the ice grains for surfaces that are both perpendicular and wider than the beam's wavelength. Surfaces smaller than the wavelength can lead to non-specular reflection and are difficult to detect. Likewise, surfaces not perpendicular to the beam will reflect at an angle and cannot be detected using a single transducer.

2.3.1 Single-element compared with multi-element transducers

A single-element transducer can only generate an ultrasonic beam in one direction, which restricts the number of angles that can be achieved due to the cylindrical shape of the ice core. In contrast, a multi-element ultrasound transducer consists of several piezoelectric elements that generate and receive ultrasound waves. By applying a time delay between the elements, beamforming can be used to angle the ultrasonic beam. In our model, the multi-element transducer has an angular range of 90°. At each azimuth scanning point around the core, we record 90 readings (one per degree), which increases the accuracy of the reflection and velocity data.

2.3.2 Reducing positional error of reflection points using ultrasonic velocities

The collected data from reflection analysis comprises solely the time-of-flight, and the position of the reflection point must be estimated based on an assumed velocity. This assumed velocity is determined by averaging the highest and lowest expected velocities (3.85 km/s).

To enhance the accuracy of the velocity prediction, a back projection technique modified for anisotropic material is employed. This method assumes that the grains have a uniform orientation (155°) with varying tilts. The velocity through the core at a specific azimuth is determined by averaging the grain velocities the beam passes through, scaled by the percentage

of the total beam distance. By utilizing the beam's angle and the grains' orientation, the tilt can be approximated using the derived velocities of the monocrystal. This information is then plotted on a grid, with each element being 0.8mm in width and height. The grid is utilized to recalculate the position of reflection points. Interestingly, the reflection point position calculation produces superior results when the velocity is applied to the grid in random order.

3 DATA ANALYSIS AND RESULTS

The present study reports on the application of back-projected velocities to determine the total number of reflection points and the average distance between the actual and predicted positions. The investigation also involves a visual examination of the reflection point images against the original crystal fabric image to ascertain their ability to reveal the grain geometry of the ice core. In Figures 3 and 4, the predicted points of reflection are denoted by red dashes, and the actual position of the reflection point is indicated by black arrows.

3.1 Single-element transducer

Table 2. The effect of scanning resolution on the total number of reflection points and the error before and after back-projected velocities are applied with a single-element transducer.

Scanning azimuth resolution (degrees)	Total reflection points	Average reflection point error before back projection (mm)	Average reflection point error after back projection (mm)
180	2	0.778	0.279
120	4	1.343	0.757
90	3	0.750	0.253
45	7	0.938	0.506
40	10	1.044	0.616
22.5	10	1.019	0.456
11.25	19	1.002	0.499
13.33	28	1.139	0.558
5.62	32	1.012	0.457
4.44	76	1.002	0.423
2.81	63	1.048	0.486
1.48	123	1.063	0.47
0.49	147	1.035	0.449

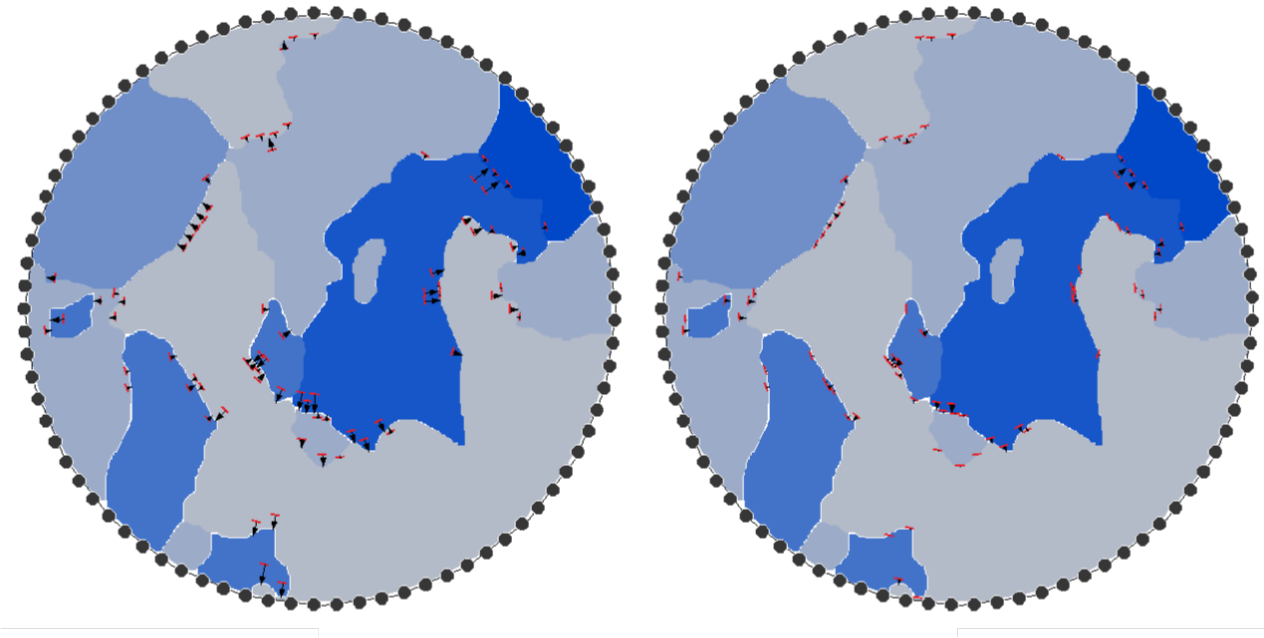

Figure 3. The simulation images of scanning resolution of 4.44° with a single-element transducer. Top-left: Reflection points without applying back projection velocities; top-right: velocity grind after back projection.

3.2 Multi-element transducer

Table 3. The effect of scanning resolution on the total number of refection points and the error before and after back-projected velocities are applied and a multi-element transducer.

Scanning azimuth angular resolution	Total reflection points	Average reflection point error before back projection (mm)	Average reflection point error after back projection (mm)
360	68	1.144	0.615
180	117	0.949	0.398
120	128	1.030	0.590
90	186	1.03	0.47
45	298	0.94	0.46
40	324	0.972	0.478
22.5	448	0.920	0.45
11.25	609	0.89	0.47
13.33	560	0.906	0.491
5.62	733	0.871	0.453
4.44	739	0.887	0.431
2.81	810	0.883	0.464

1.48	846	0.871	0.445
0.49	919	0.899	0.473

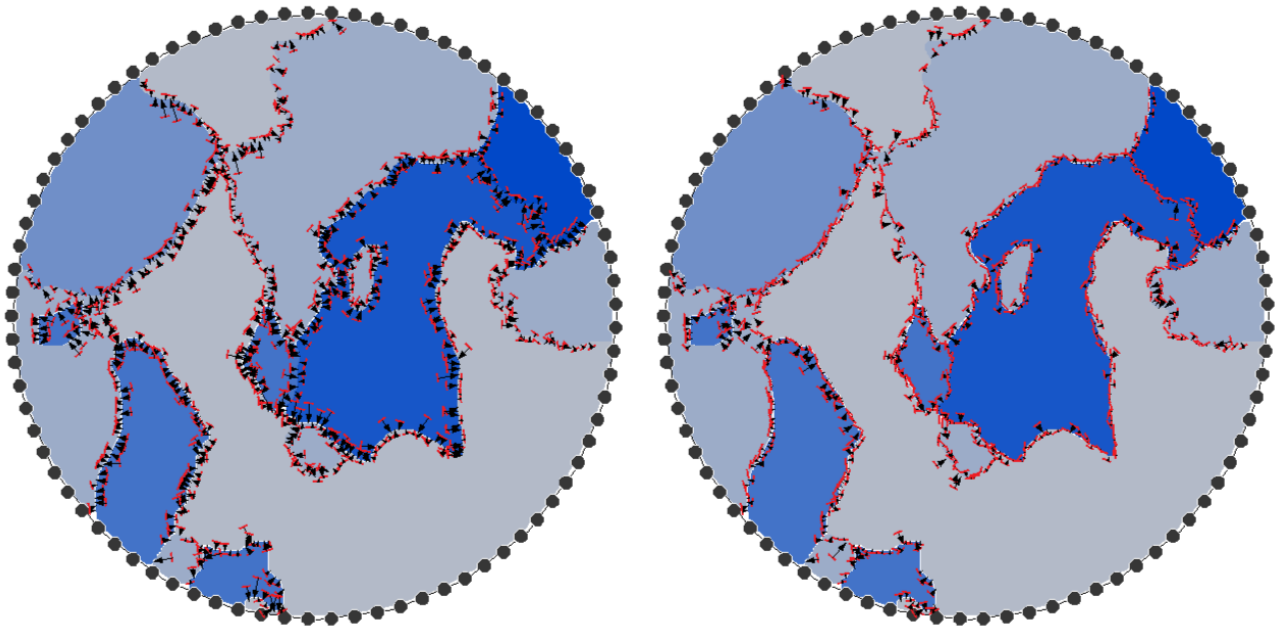

Figure 4. Simulation of scanning resolution of $4.44°$ with a multi-element transducer. Top-left: Reflection points without applying back projection velocities; top-right: Reflection points applying back projection velocities.

4 . CONCLUSIONS

Through visual analysis of the reflection points, it became evident that a single-element transducer cannot provide sufficient coverage to accurately reconstruct the ice core's grain geometry. A minimum of approximately 300 reflection points is required for a comprehensive image of the grain structure. However, a multi-element transducer equipped with beamforming and a scanning resolution of $40°$ is capable of revealing the intricate details of the grain geometry.

Typically, when an assumed velocity is used, the positional error of reflection points is $\approx 1\,\mathbf{mm}$. However, increasing azimuth scanning resolution can help mitigate this error. By utilising velocity data, the positional error of reflection points can be reduced by an average of 55.5%. Additionally, reducing the scanning resolution results in a decrease in the positional error of reflection points.

When using a multi-element transducer, the benefits of increasing scanning resolution for recreating grain geometry are subject to diminishing returns beyond $40°$. At low scanning resolutions ($13.33°$-$0.49°$), the correlation between reflection point error correction and scanning resolution diminishes, which is most likely attributable to the resolution of the velocity grid (0.8 mm). While the tilt assumptions using the multi-element transducer are

similar to the actual tilt of the core, further improvements could be achieved through the incorporation of filtering techniques.

With a muli-element transducer, there are diminishing returns above a 40° scanning resolution when recreating grain geometry. At low scanning resolutions (13.33°-0.49°), the reflection point error correction loses its correlation with scanning resolution. This is most likely due to the resolution of the velocity grid (0.8mm). With the multi-element transducer, the tilt assumptions are similar to the actual tilt of the core. This could be improved by adding filtering.

The findings of this study suggest that reflection data may be utilised for reconstructing the grain geometry of deep ice cores with single maximum fabrics. With a precise grain geometry, determining the grains' tilt using iterative reconstruction becomes more efficient, as solutions for each defined grain are required rather than for numerous grid points.

In this simulation, we make many assumptions. The derived monocrystal velocities are higher than the measured velocities of ice. Natural ice has impurities and is porous. Both of these properties reduce the velocity of p-waves through the ice. The presence of large bubbles also adds points of non-specular reflection; this would interfere with the measurement of reflection points.

The sample utilised in this study consisted of deep ice featuring predominantly vertical grains with unidirectional grain orientation. This specific grain arrangement was necessary for the implementation of the back projection technique, as multiple combinations of tilts and orientations can yield equivalent p-wave velocities.

In upcoming simulation iterations, crystal fabrics from various sources will be employed. The simulation framework will be extended to account for attenuation and non-specular reflection phenomena resulting from the presence of gas bubbles within the ice matrix. The validity of these simulations will be assessed through experimentation involving artificial ice cores, which will be subjected to ultrasound measurements and compared against polarised light microscopy imagery.

REFERENCES

Cao, P., Wu, J., Zhang, Z., Fang, B., Peng, L., Li, T., Vlugt, T. J. H. and Ning, F. (2018) Mechanical properties of bi- and poly-crystalline ice, *AIP Advances,* 8 (12), pp. 125108-125108. DOI: 10.1063/1.5042725.

Cole, D. M. (1998) Modeling the cyclic loading response of sea ice, *International Journal of Solids and Structures,* 35 (31-32), pp. 4067. DOI: 10.1016/s0020-7683(97)00301-6.

Diez, A. and Eisen, O. (2015) Seismic wave propagation in anisotropic ice – Part 1: Elasticity tensor and derived quantities from ice-core properties, *The Cryosphere,* 9 (1), pp. 367. DOI: 10.5194/tc-9-367-2015.

Durand, G., Gagliardini, O., Thorsteinsson, T., Svensson, A., Kipfstuhl, S. and Dahl-Jensen,

D. (2006) Ice microstructure and fabric: An up-to-date approach for measuring textures, *Journal of Glaciology,* 52 (179), pp. 619-630. DOI: 10.3189/172756506781828377.

Gillet-Chaulet, F., Gagliardini, O., Meyssonnier, J., Montagnat, M. and Castelnau, O. (2005) A user-friendly anisotropic flow law for ice-sheet modeling, *Journal of Glaciology,* 51 (172), pp. 3-14. DOI: 10.3189/172756505781829584.

Hellmann, S., Grab, M., Kerch, J., Löwe, H., Bauder, A., Weikusat, I. and Maurer, H. (2021) Acoustic velocity measurements for detecting the crystal orientation fabrics of a temperate ice core, -02-04, . DOI: 10.5194/tc-2021-7.

Hellmann, S., Kerch, J., Weikusat, I., Bauder, A., Grab, M., Jouvet, G., Schwikowski, M. and Maurer, H. (2021) Crystallographic analysis of temperate ice on rhonegletscher, swiss alps, *The Cryosphere,* 15 (2), pp. 677-694. DOI: 10.5194/tc-15-677-2021.

Kennedy, J. H., Pettit, E. C. and Di Prinzio, C. L. (2013) The evolution of crystal fabric in ice sheets and its link to climate history, *Journal of Glaciology,* 59 (214), pp. 357-373. DOI: 10.3189/2013JoG12J159.

Kerch, J., Diez, A., Weikusat, I. and Eisen, O. (2018) Deriving seismic velocities on the micro-scale from c-axis orientations in ice cores, -01-04, . DOI: 10.5194/tc-2017-281.

Langway, C. C., Shoji, H. and Azuma, N. (1988) Crystal size and orientation patterns in the wisconsin-age ice from dye 3, greenland, *Annals of Glaciology,* 10 , pp. 109-115. DOI: 10.3189/S0260305500004262.

Mikesell, T. D., Van Wijk, K., Otheim, L. T., Marshall, H. and Kurbatov, A. (2017) Laser Ultrasound Observations of Mechanical Property Variations in Ice Cores, *Geosciences,* -06-24, 7 (3). DOI: 10.3390/geosciences7030047.

Placidi, L., Greve, R., Seddik, H. and Faria, S. H. (2010) Continuum-mechanical, anisotropic flow model for polar ice masses, based on an anisotropic flow enhancement factor, *Continuum Mechanics and Thermodynamics,* 22 (3), pp. 221-237. DOI: 10.1007/s00161-009-0126-0.

Saruya, T., Fujita, S., Iizuka, Y., Miyamoto, A., Ohno, H., Hori, A., Shigeyama, W., Hirabayashi, M. and Goto-Azuma, K. (2022) Development of crystal orientation fabric in the dome fuji ice core in east antarctica: Implications for the deformation regime in ice sheets, *The Cryosphere,* 16 (7), pp. 2985-3003. DOI: 10.5194/tc-16-2985-2022.

Simonetti, F. and Fox, M. (2019) Experimental methods for ultrasonic testing of complex-shaped parts encased in ice, *NDT & E International : Independent Nondestructive Testing and Evaluation,* 103 , pp. 1-11. DOI: 10.1016/j.ndteint.2019.01.008.

Tsvankin, I. (2012) Seismic Signatures and Analysis of Reflection Data in Anisotropic Media, Third edition , pp. 14–35 . DOI: 10.1190/1.9781560803003.